Electronic Supplementary Material

Structural spectroscopic study of dissociative anaesthetic methoxphenidine

Bronislav Jurásek*[a], Patrik Fagan[b], Bohumil Dolenský[b], Natalie Paškanová[a], Kristýna Dobšíková[b], Ivan Raich[d], Radek Jurok[a,c], Vladimír Setnička[b], Michal Kohout[c], Jan Čejka,[e] Martin Kuchař[a].

[a] Forensic Laboratory of Biologically Active Substances, Department of Chemistry of Natural Compounds, University of Chemistry and Technology Prague, Technická 5, 166 28 Praha, Czech Republic

[b] Department of Analytical Chemistry, University of Chemistry and Technology Prague, Technická 5, 166 28 Praha, Czech Republic

[c] Department of Organic Chemistry, University of Chemistry and Technology Prague, Technická 5, 166 28 Praha, Czech Republic

[d] Department of Chemistry of Natural Compounds, University of Chemistry and Technology Prague, Technická 5, 166 28 Praha, Czech Republic

[e] Department of Solid State Chemistry, University of Chemistry and Technology Prague, Technická 5, 166 28 Praha, Czech Republic

Enantiomeric purity of methoxphenidine controlled by HPLC

For the purity control of the enantiomers obtained by crystallization, the method from Taschwer et al. has been used. This chromatographic method using a Lux® Cellulose-2 column achieved the highest resolution among other published methods on the chiral resolution of MXP in HPLC. The selected method was transferred to our chromatographic system, which can be operated not only in SFC, but also in pure HPLC mode. The wavelength of the detector was set to 276 nm based on the absorption maximum of MXP. The first eluted peak was assigned as MXP-b, the second one as MXP-a. The retention time of the enantiomers of MXP was $t_{MXP\text{-}b}$ = 19.46 min and $t_{MXP\text{-}a}$ = 34.41 min, the resolution factor was approximately 12.07 (Figure S1).

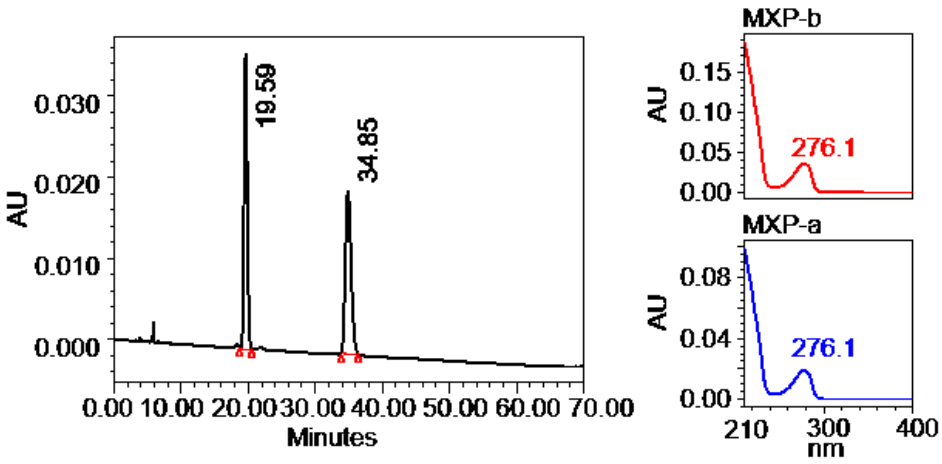

Figure S1: The HPLC chromatogram of MXP enantioseparation and UV spectra of its enantiomers. The analysis was performed on a Lux® Cellulose-2 (250 × 4.6 mm, 5 µm) using a mobile phase composed of acetonitrile/propan-2-ol/diethylamine/formic acid (95/5/0.1/0.1; v/v/v/v) at a flow rate of 1 mL min^{-1}. The temperature was set at 27 °C and the injection volume was 5 µL at a sample concentration of 1 mg mL^{-1}.

We were able to determine the purity of the enantiomers during the crystallization process. The final purity of MXP enantiomers was determined from the ratio of peaks area (Figure S2). Enantiomeric purity of MXP-b was 99.42 % and that of MXP-a was 99.50 %. However, it should be noted that, we encountered a problem connected with the impurity coming from the crystallization. We identified the impurity as (+)-2,3-dibenzoyl-D-tartaric acid monohydrate (t = 47.69 min) in case of MXP-b. There is a small baseline disturbance in the vicinity of the peak MXP-a, which prevents the determination of its purity with accuracy. This baseline disturbance was concluded as elution of (–)-2,3-dibenzoyl-L-tartaric acid monohydrate.

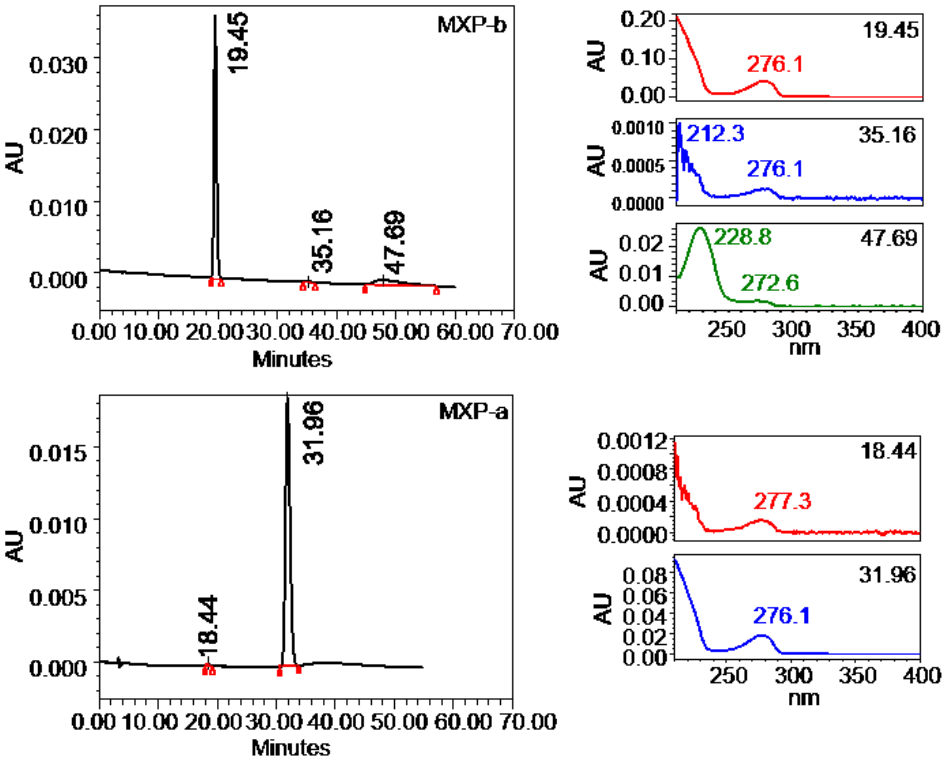

Figure S2: The HPLC determination of the enantiomeric purity of the MXP enantiomers. The analysis was performed on a Lux® Cellulose-2 (250 × 4.6 mm, 5 µm) using a mobile phase composed of acetonitrile/propan-2-ol/diethylamine/formic acid (95/5/0.1/0.1; v/v/v/v) at a flow rate of 1 mL min^{-1}. The temperature was set at 27 °C and the injection volume was 5 µL at a sample concentration of 1 mg mL^{-1}.

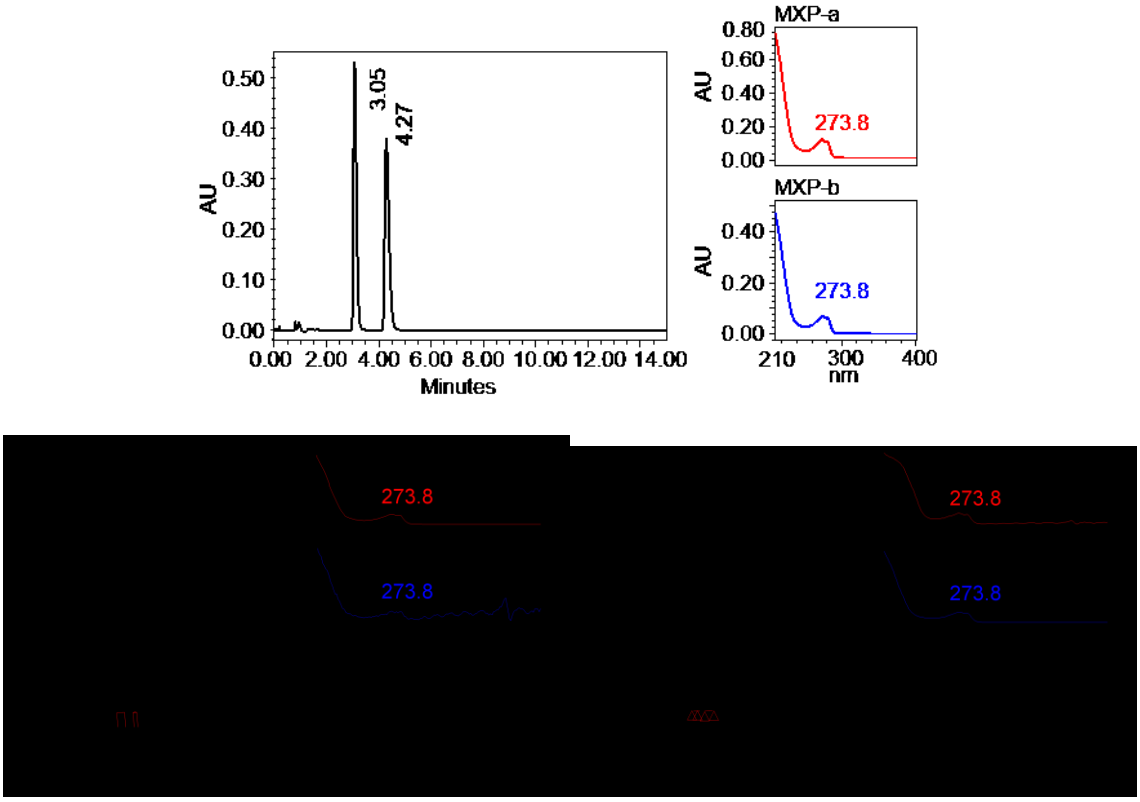

Figure S3: The SFC determination of the enantiomeric purity of the MXP enantiomers. A CHIRALPAK® IE-3 column with a mobile phase composed of CO_2/propan-2-ol/isopropylamine (60/40/0.1, v/v/v). The flow rate was set to 1 mL min^{-1}, temperature to 35 °C, and ABPR to 2500 psi (172 bar). Detection wavelengths were 220 and 254 nm. Injection volume was 2 µL.

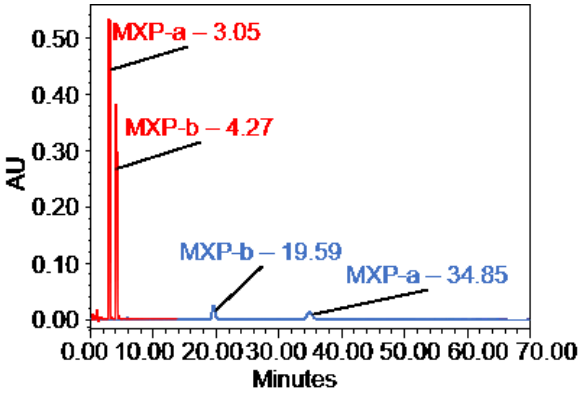

Figure S4: The HPLC (blue line) and the new SFC (red line) method of the MXP enantioseparation. Chromatographic conditions for the chiral resolution of MXP enantiomers in HPLC and SFC are identical as above.

Optimization of SFC enantioseparation

Table S1: Data describes the effect of mobile phase composition on elution time (t_1, t_2), selectivity (α) and resolution (R); "x" means no elution in 150 minutes, "-" means no chiral separation

Alcyon SFC CSP Amylose-SA									
MP	**t_1 [min]**	**t_2 [min]**	**α**	**R**	**MP**	**t_1 [min]**	**t_2 [min]**	**α**	**R**
CO_2/propan-2-ol/isopropylamine (v/v/v)					CO_2/ethanol/isopropylamine (v/v/v)				
90/10/0.1	**2.40**	**3.15**	**1.47**	**3.24**	90/10/0.1	2.63	-	-	-
CO_2/propan-2-ol/diethylamine (v/v/v)					CO_2/ethanol/diethylamine (v/v/v)				
90/10/0.1	2.30	2.96	1.44	3.20	90/10/0.1	2.74	-	-	-
CO_2/propan-2-ol/formic acid (v/v/v)					CO_2/ethanol/formic acid (v/v/v)				
90/10/0.1	14.70	-	-	-	90/10/0.1	9.60	-	-	-
CO_2/propan-2-ol/diethylamine/formic acid (v/v/v/v)					CO_2/ethanol/diethylamine/formic acid (v/v/v/v)				
90/10/0.1/0.1	**5.08**	**12.46**	**2.71**	**11.00**	90/10/0.1/0.1	4.97	5.40	1.10	1.12
CO_2/methanol/isopropylamine (v/v/v)					CO_2/acetonitrile/isopropylamine (v/v/v)				
90/10/0.1	3.72	-	-	-	90/10/0.1	2.61	-	-	-
CO_2/methanol/diethylamine (v/v/v)					CO_2/acetonitrile/diethylamine (v/v/v)				
90/10/0.1	3.37	-	-	-	90/10/0.1	2.66	-	-	-
CO_2/methanol/formic acid (v/v/v)					CO_2/acetonitrile/formic acid (v/v/v)				
90/10/0.1	8.60	-	-	-	90/10/0.1	x	x	x	x
CO_2/methanol/diethylamine/formic acid (v/v/v/v)					CO_2/acetonitrile/diethylamine/formic acid (v/v/v/v)				
90/10/0.1/0.1	3.80	-	-	-	90/10/0.1/0.1	34.26	46.37	1.36	1.52

Alcyon SFC CSP Cellulose-SB									
MP	**t_1 [min]**	**t_2 [min]**	**α**	**R**	**MP**	**t_1 [min]**	**t_2 [min]**	**α**	**R**
CO_2/propan-2-ol/isopropylamine (v/v/v)					CO_2/ethanol/isopropylamine (v/v/v)				
90/10/0.1	2.59	-	-	-	90/10/0.1	2.58	-	-	-
CO_2/propan-2-ol/diethylamine (v/v/v)					CO_2/ethanol/diethylamine (v/v/v)				
90/10/0.1	2.59	-	-	-	90/10/0.1	2.55	-	-	-
CO_2/propan-2-ol/formic acid (v/v/v)					CO_2/ethanol/formic acid (v/v/v)				
90/10/0.1	15.02	-	-	-	90/10/0.1	7.20	-	-	-
CO_2/propan-2-ol/diethylamine/formic acid (v/v/v/v)					CO_2/ethanol/diethylamine/formic acid (v/v/v/v)				
90/10/0.1/0.1	4.55	-	-	-	90/10/0.1/0.1	4.16	-	-	-
CO_2/methanol/isopropylamine (v/v/v)					CO_2/acetonitrile/isopropylamine (v/v/v)				
90/10/0.1	2.89	-	-	-	90/10/0.1	3.29	-	-	-
CO_2/methanol/diethylamine (v/v/v)					CO_2/acetonitrile/diethylamine (v/v/v)				
90/10/0.1	2.74	-	-	-	90/10/0.1	3.45	-	-	-
CO_2/methanol/formic acid (v/v/v)					CO_2/acetonitrile/formic acid (v/v/v)				
90/10/0.1	12.60	-	-	-	90/10/0.1	x	x	x	x
CO_2/methanol/diethylamine/formic acid (v/v/v/v)					**CO_2/acetonitrile/diethylamine/formic acid (v/v/v/v)**				
90/10/0.1/0.1	3.07	-	-	-	**90/10/0.1/0.1**	**17.16**	**18.44**	**1.08**	**1.05**

Alcyon SFC CSP Cellulose-SC									
MP	**t_1 [min]**	**t_2 [min]**	**α**	**R**	**MP**	**t_1 [min]**	**t_2 [min]**	**α**	**R**
CO_2/propan-2-ol/isopropylamine (v/v/v)					CO_2/ethanol/isopropylamine (v/v/v)				
90/10/0.1	10.84	12.18	1.13	1.63	90/10/0.1	15.55	-	-	-
CO_2/propan-2-ol/diethylamine (v/v/v)					**CO_2/ethanol/diethylamine (v/v/v)**				
90/10/0.1	**11.06**	**12.46**	**1.14**	**1.68**	**90/10/0.1**	**14.45**	**16.62**	**1.16**	**2.73**
CO_2/propan-2-ol/formic acid (v/v/v)					CO_2/ethanol/formic acid (v/v/v)				
90/10/0.1	x	x	x	x	90/10/0.1	94.00	-	-	-
CO_2/propan-2-ol/diethylamine/formic acid (v/v/v/v)					CO_2/ethanol/diethylamine/formic acid (v/v/v/v)				
90/10/0.1/0.1	x	x	x	x	90/10/0.1/0.1	42.21	47.00	1.12	2.55
CO_2/methanol/isopropylamine (v/v/v)					CO_2/acetonitrile/isopropylamine (v/v/v)				
90/10/0.1	21.28	22.76	1.07	1.29	90/10/0.1	4.16	-	-	-
CO_2/methanol/diethylamine (v/v/v)					CO_2/acetonitrile/diethylamine (v/v/v)				
90/10/0.1	**20.59**	**22.00**	**1.07**	**1.38**	90/10/0.1	3.22	-	-	-
CO_2/methanol/formic acid (v/v/v)					CO_2/acetonitrile/formic acid (v/v/v)				
90/10/0.1	x	x	x	x	90/10/0.1	x	x	x	x
CO_2/methanol/diethylamine/formic acid (v/v/v/v)					CO_2/acetonitrile/diethylamine/formic acid (v/v/v/v)				
90/10/0.1/0.1	29.08	-	-	-	90/10/0.1/0.1	x	x	x	x

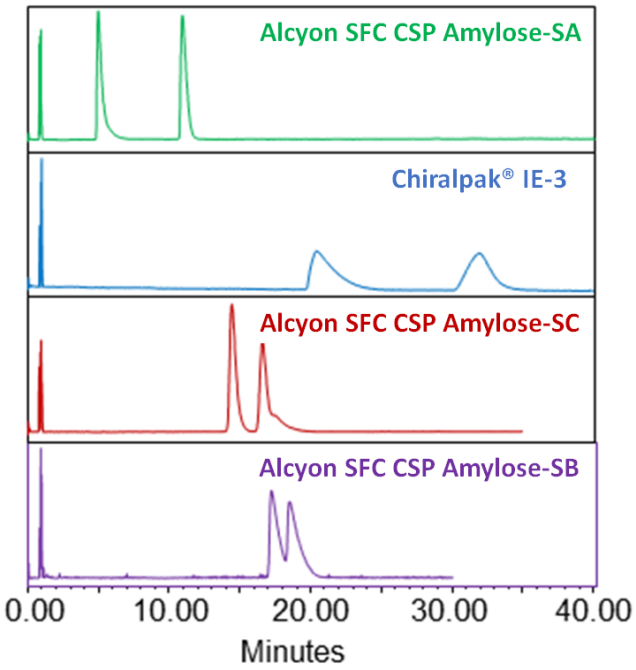

Figure S5: The chromatograms showing the highest resolution for individual columns; mobile phases are listed in Table S1, and Table 2, line 4 for Chiralpak IE-3. Namely, An Alcyon SFC CSP Amylose-SA with a mobile phase CO_2/propan-2-ol/diethylamine/formic acid (90/10/0.1/0.1, v/v/v/v), a CHIRALPAK® IE-3 column with a mobile phase composed of CO_2/propan-2-ol/isopropylamine (60/40/0.1, v/v/v), an Alcyon SFC CSP Cellulose-SC with a mobile phase CO_2/ethanol/diethylamine (90/10/0.1, v/v/v) and an Alcyon SFC CSP Cellulose-SB with a mobile phase CO_2/acetonitrile/diethylamine/formic acid (v/v/v/v, 90/10/0.1/0.1). The chromatographic measurements were performed at a flow rate of 1 mL min^{-1}, temperature 35 °C; the ABPR was set to 2500 psi (172 bar) and detection wavelengths to 220 and 254 nm. Injection volume was 2 µL.

Table S2: The Effect of the ratio of carbon dioxide and a modifier with additives on the elution time (t_1, t_2), selectivity (α) and resolution (R)

CHIRALPAK® IE-3				
MP	**t_1 [min]**	**t_2 [min]**	**α**	**R**
CO_2/propan-2-ol/isopropylamine (v/v/v)				
60/40/0.1	**3.19**	**4.59**	**1.53**	**5.26**
70/30/0.1	5.13	6.82	1.39	3.35
80/20/0.1	9.53	12.51	1.34	2.81
90/10/0.1	20.38	31.92	1.59	3.78

Alcyon SFC CSP Amylose-SA				
MP	**t_1 [min]**	**t_2 [min]**	**α**	**R**
CO_2/propan-2-ol/diethylamine/formic acid (v/v/v/v)				
60/40/0.1/0.1	1.27	2.57	3.72	7.14

70/30/0.1/0.1	1.61	3.78	3.68	10.62
80/20/0.1/0.1	**2.46**	**6.53**	**3.44**	**13.99**
90/10/0.1/0.1	**4.81**	**14.38**	**3.38**	**12.86**
95/5/0.1/0.1	23.80	10.22	2.44	6.51
98.5/2.5/0.1/0.1	25.13	46.28	1.87	3.82

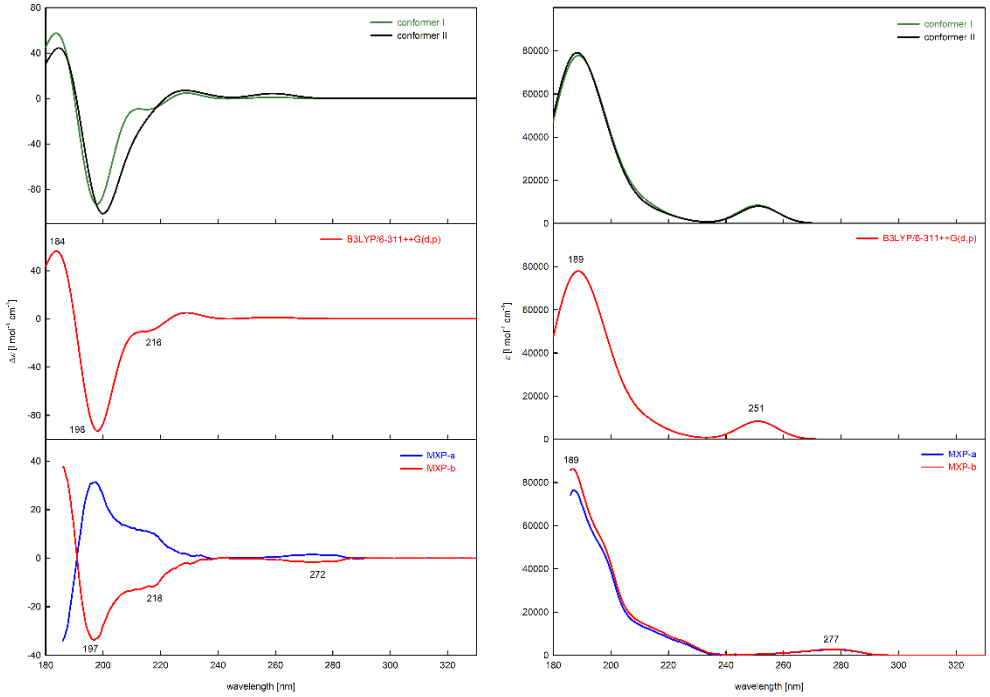

Figure S6: The ECD spectra (left) and the UV absorption spectra (right) of (*R*)-MXP hydrochloride. The simulated spectra of individual conformers at the B3LYP/6-311++G(d,p) level (top), their Boltzmann-weighted spectra (middle) and the experimental spectra of both enantiomers (bottom). The spectra were displayed in the spectral range of 185–330 nm.

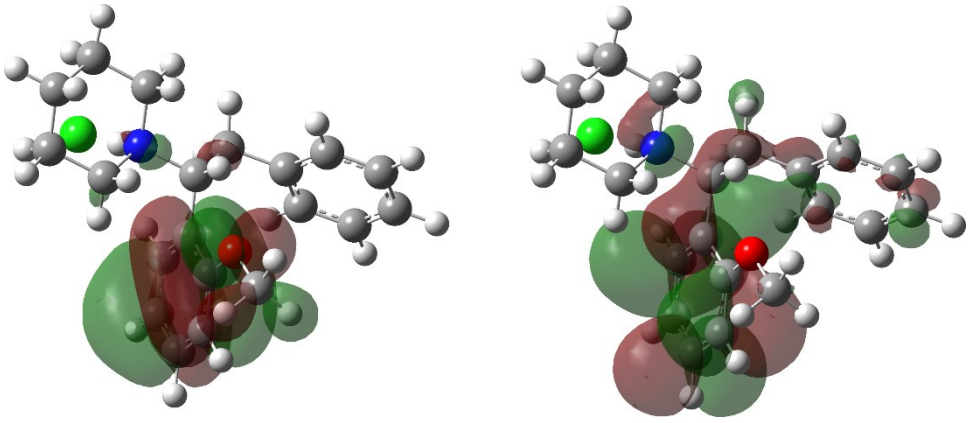

Figure S7: The electronic transitions from the highest occupied orbital (HOMO, left) to the lowest unoccupied molecular orbital (LUMO, right) of the most abundant conformer of (*R*)-MXP hydrochloride simulated at B3LYP/6-311++G(d,p) level.

Table S3: The crystal data and details of the structure determination for: MXP-N2-V7 (P 21 21 21, R = 0.03)

Crystal Data

Formula	**C20 H26 Cl1 N1 O1**
Formula Weight	331.88
Crystal System	orthorhombic
Space group	P212121 (No. 19)
a, b, c [Angstrom]	9.3989(4) 10.3835(4) 37.4316(15)
V [Ang3]**	3653.1(3)
Z	8
D(calc) [g/cm3]**	1.207
Mu(CuKa) [/mm]	1.868
F(000)	1424
Crystal Size [mm]	0.02 x 0.12 x 0.27

Data Collection

Temperature (K)	**180**
Radiation [Angstrom]	CuKa 1.54180
Theta Min-Max [Deg]	2.4, 68.2
Dataset	-11: 11 ; 0: 12 ; 0: 44
Tot., Uniq. Data, R(int)	42650, 6649, 0.045
Observed Data [I > 2.0 sigma(I)]	6277

Refinement

Nref, Npar	**6648, 424**
R, wR2, S	0.0330, 0.0894, 0.98
w = = MODIFIED SHELDRICK W=1/[\S^2^(F^2^) + (0.05P)^2^ + 1.02P]	
Max. and Av. Shift/Error	0.00, 0.00
Flack x	-0.012(10)
Min. and Max. Resd. Dens. [e/Ang^3]	-0.15, 0.16

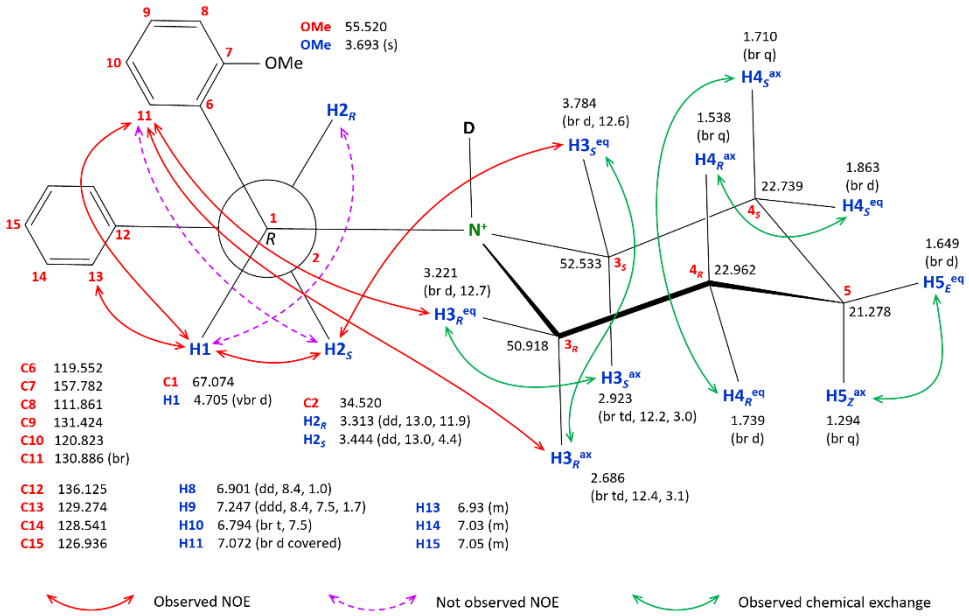

Figure S8: The average MXP.HCl conformation derived based on the NMR characteristics (D_2O at 22°C)

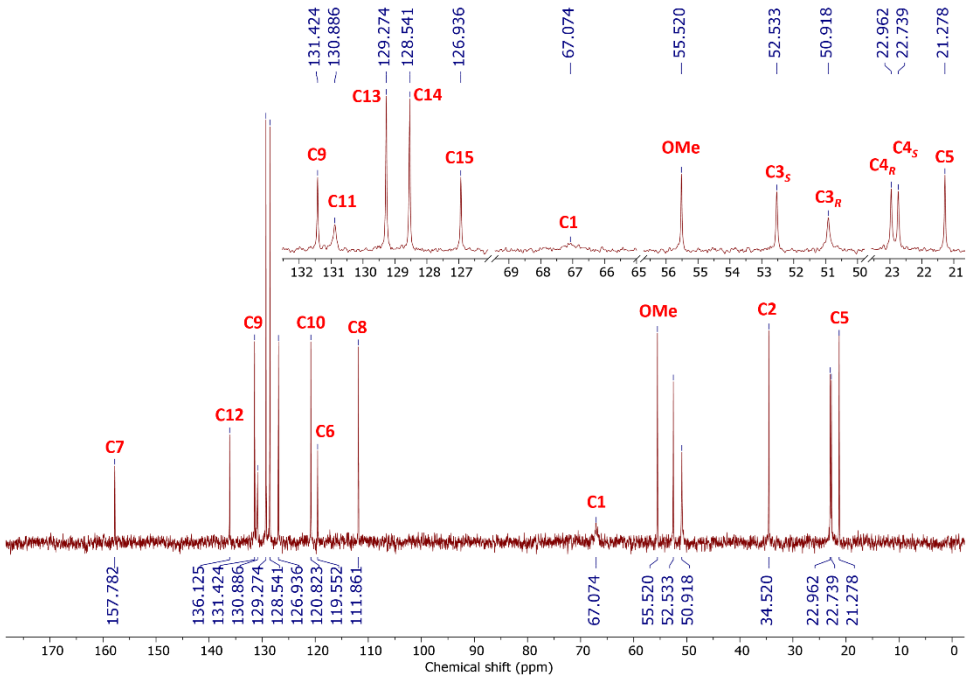

Figure S9: The ^{13}C NMR (126 MHz, D_2O, 22°C) spectrum of MXP.HCl

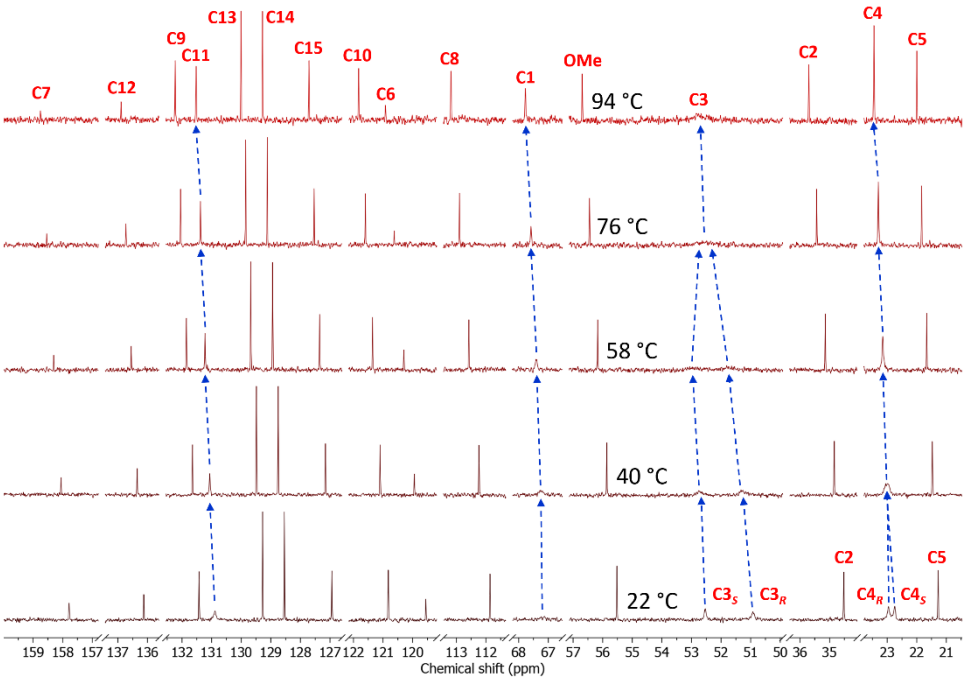

Figure S10: The ^{13}C NMR (126 MHz, D_2O) spectra of MXP.HCl at various temperatures

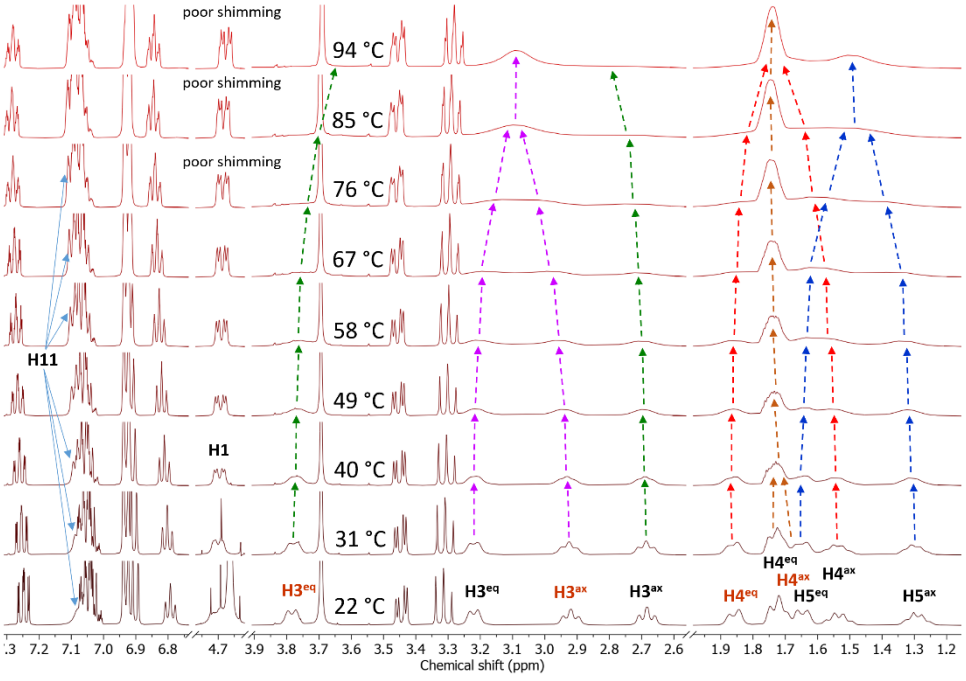

Figure S11: The ^{1}H NMR (500 MHz, D_2O) spectra of MXP.HCl at various temperatures

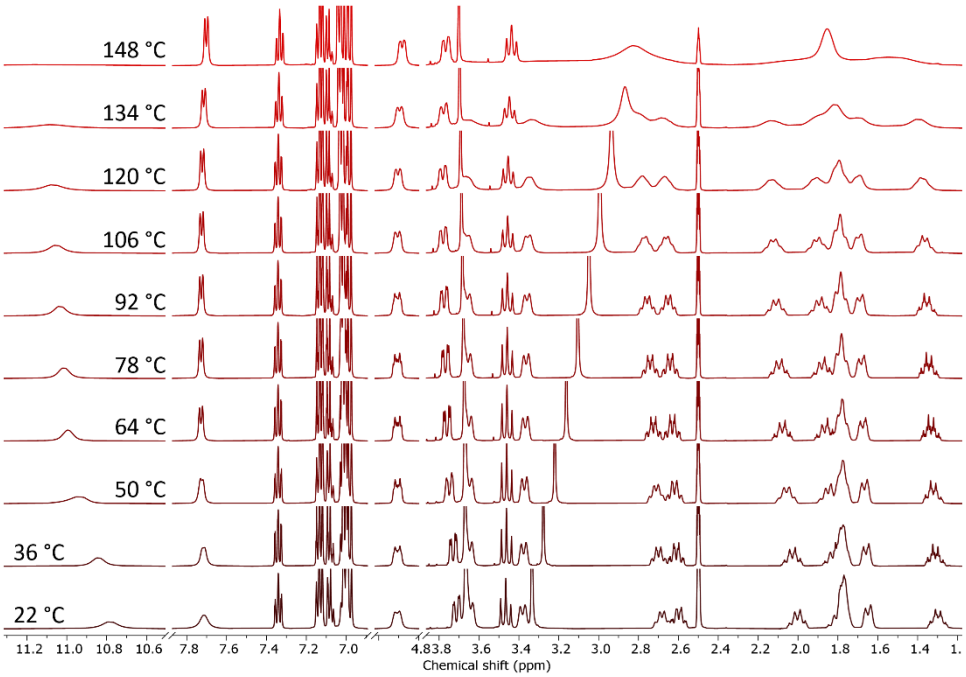

Figure S12: The ^{1}H NMR (500 MHz, DMSO-d_6) spectra of MXP.HCl at various temperatures

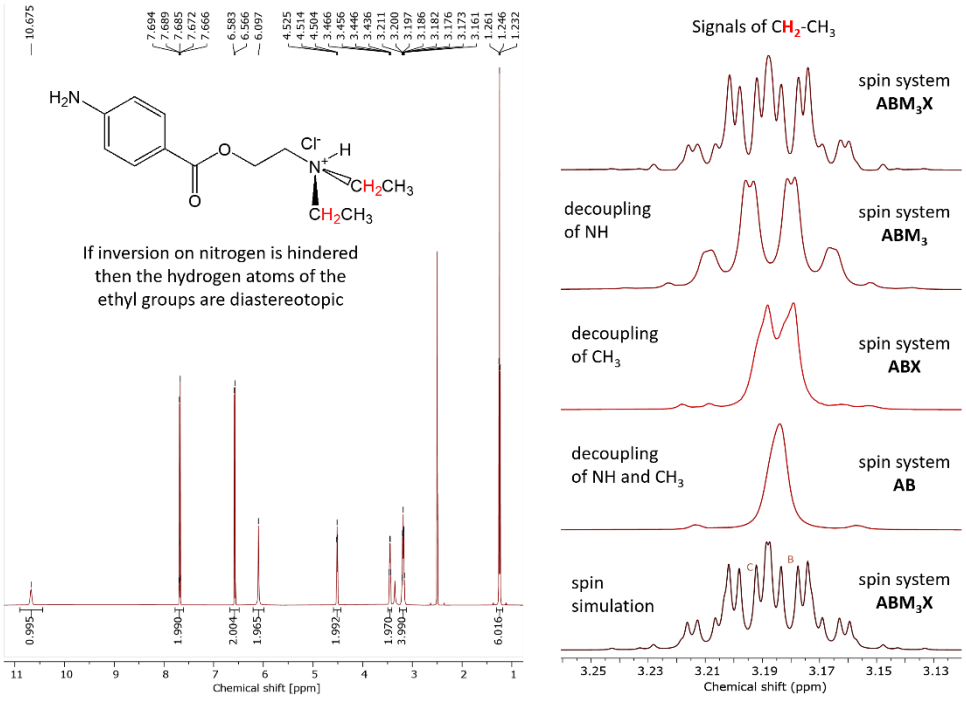

Figure S13: The ^{1}H NMR (500 MHz) spectra of procaine hydrochloride